Miniaturized Frequency Selective Rasorber Based on Meander-Lines Loaded Lumped Resistors and a Coupled Resonator Spatial Filter

Zhaoshuzhou Shen, Na Kou, Shixing Yu, Zhao Ding, and Zhengping Zhang[*]

Abstract—This paper presents a miniaturized frequency selective rasorber (FSR) with both wide absorption and transmission bands. The proposed FSR consists of a resistive sheet and a band-pass frequency-selective surface (FSS) with non-resonant constituting elements. The unit cell structure of the resistive sheet is a meander line loaded with four lumped resistors, which generate a wide absorption band from 2.4 to 6.2 GHz, while the layer of FSS is coupled resonator spatial filter (CRSF) that generates a wide transmission band from 7.5 to 10.2 GHz. Furthermore, there is a 10.5 mm air spacer between the resistive and FSS layers. The period of the FSR structure, which maintains its passband and absorption band performance, is only 10 mm ($0.08\lambda_L$). Simulated and measured results are compared and found to show good agreement.

1. INTRODUCTION

The frequency-selective surface (FSS) is an array of periodic structures composed of either metallic patches or a conducting screen perforated with apertures attached on a substrate [1]. It shows the characteristics of a spatial filter, having bandpass or bandstop response when the electromagnetic wave is incident upon it. The FSSs have a wide spectrum of applications in many fields, such as military, wireless communication, medical apparatus and instruments, aeronautics and astronautics, high-power microwave systems [2]; this technology has been widely applied in radomes [3, 4], antennas [5, 6], metamaterials [7, 8], polarizers [9, 10], and other applications. In 2010, a generalized method for frequency selective surfaces with non-resonant constituting elements was proposed by Al-Joumayly and Behdad [14]. This type of FSS has a small period, sharp frequency selectivity, wide passband, and stable frequency responses. Three years later, the coupled resonator spatial filter (CRSF) was proposed. It changed the metallic grid of the FSS with non-resonant constituting elements into metallic circular-aperture square. The CRSF shows more stable performances with different polarization states and angles of incident wave [15].

However, the traditional FSS radome can only reduce the mono-static RCS of the antenna. In other directions, it still has a strong out-of-band reflection, which results in an increased RCS. Hence, the traditional FSSs may be detected by bistatic or multi-static radars [12]. Therefore, a new ideal radome was proposed to compensate this deficiency, which is nearly transparent at the passband while the wave can be absorbed by the structure out of the passband. This new structure is named as frequency-selective rasorber (FSR) [16]. The word "rasorber" is the combination of "radome" and "absorber", and is a type of radome that functions as an absorber [11]. The FSR is a rasorber that has a transmission and an absorption band, retaining the advantages of the FSS and the absorber, while the FSS only shows the characteristics of spatial filter and cannot absorb out-of-band total reflection of the incident wave.

* Corresponding author: Zhengping Zhang (zpzhang@gzu.edu.cn).
The authors are with the Big Data and Electronics Engineering Department, Guizhou University, Guiyang, China.

Existing FSRs are usually classified into two types according to their structures, 2-D FSR [11, 12] and 3-D FSR [13]. 2-D FSR is usually composed of a lossy sheet and a traditional band-pass FSS. At the passband, both layers are in resonance, so the FSR is nearly transparent, while at the stopband, the band-pass FSS is equal to a plate metal, and the entire FSR structure acts as a Salisbury screen [18].

In this paper, a miniaturized frequency selective rasorber was proposed. It has a simplified structure, which is based on meander lines loaded with lumped resistors while maintaining the performance of frequency selectivity and out-of-band absorption.

Section 2 gives the specific design of the proposed FSR. Section 3 describes the manufactured prototype of the proposed FSR and compares the simulated and measured results. Finally, in Section 4 the conclusion is presented.

2. DESIGN OF THE FSR

Equivalent transmission-line network of the dual-layered FSR is shown in Fig. 1. Z_0, Z_1, Z_2 are the impedance of the air, resistive sheet, and FSS, respectively. By analyzing the network, transmission coefficient $|S_{21}|$ and reflection coefficient $|S_{11}|$ can be expressed as

$$S_{11} = \frac{P + j(Z_1 - Z_2 - Z_0)\tan\theta}{P + 2Q/Z_0 + j(Z_0 + P + 2Q/Z_0)\tan\theta} \tag{1}$$

$$S_{21} = \frac{2Q}{(Z_0 P + 2Q)\cos\theta + j\left[Z_0\left(Z_0 + P\right) + 2Q\right]\sin\theta} \tag{2}$$

where $P = Z_1 + Z_2$, $Q = Z_1 Z_2$, $\theta = \beta h_1 = 2\pi f h_1/c$, c is the speed of light in vacuum, and f is the operating frequency [17].
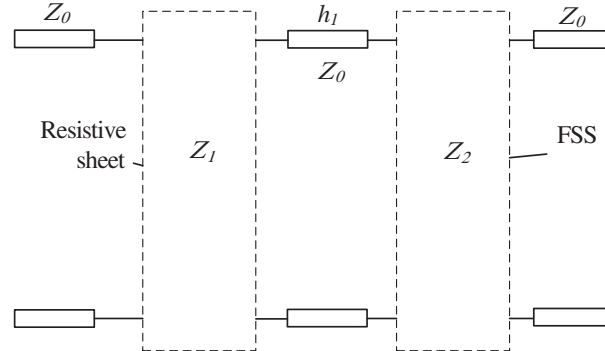
Figure 1. Equivalent transmission-line network of the dual-layered FSR.

At the transmission band, the resonant element of the resistive sheet and FSS are nearly transparent for the incident wave, and the lumped resistor does not work. It can be concluded that the loaded resistor only affects the absorption performance of the FSR. At the transmission band, the impedance of the resistive sheet Z_1 and the impedance of the FSS Z_2 go to infinity. Refer to Eqs. (1) and (2), $|S_{11}| \rightarrow 0$, $|S_{21}| \rightarrow 1$.

Based on the above analysis, the value of the lumped resistor only affects the absorption performance of the FSR, while the metal structures determine the passband performance. For reducing reflection, the real part of the Z_1 should be around Z_0. Evidently, it is equal to R. As the passband performance of the FSR is only determined by the metal structures of resistive sheet and FSS, choosing the resistive sheet/FSS with wide bandwidth of passband is a feasible method to obtain broadband FSR.

The meander line is a common structure to reduce the size of the unit cell [23, 24]. In this study, the meander line covers the entire unit as much as possible to obtain a higher inductance and fully reduce the unit size. Fig. 2 shows the structure of the meander line without lumped resistors. Figs. 3(a)–(d) illustrate the effects of the length/width of the meander line on the performance of the frequency
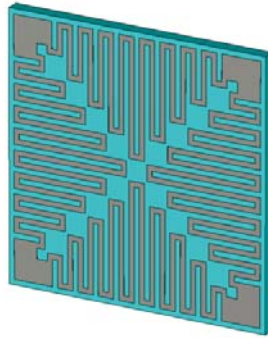
Figure 2. Structure of the meander line without lumped resistors.
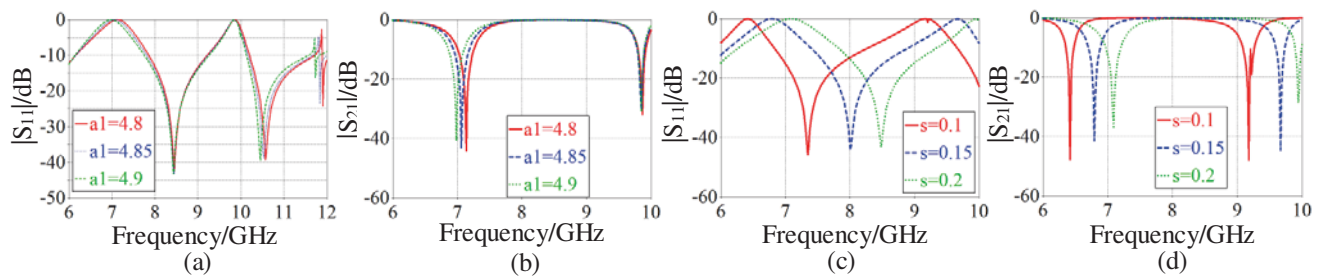
Figure 3. Simulated S-parameters of the meander line without lumped resistors (a) $|S_{11}|$ and (b) $|S_{21}|$ for different side lengths of the square a_1. (c) $|S_{11}|$ and (d) $|S_{21}|$ for different the widths of the meander line w_1.

selectivity. When a_1 is 4.9 mm and s is 0.2 mm, the 3 dB bandwidth is 2.5 GHz which is from 7.3 to 9.8 GHz. As the lengths of the square a_1 or the width of the meander line w_1 increase, the passband moves toward the high frequency, and the bandwidth decreases.

To cover the passband of the resistive sheet, a CRSF is presented. Compared with other FSSs such as square loop, cross, dipole, and FSS with non-resonant constituting elements, the CRSF has smaller period, sharper frequency selectivity, and more stable performances under different polarization states and angles of incident wave. Both resistive sheet and CRSF with broadband passband provide the proposed FSR with a wide transmission band.

Figure 4 shows the geometric topology of the proposed FSR. It is composed of a resistive sheet, an FSS, and an air space in between. The resistive sheet consists of four meander lines connected to each other by four film resistors. The resistance of each lumped resistor is 270 Ω. The width of the meander line w_1 and the width of the gap between the lines s_1 are both 0.2 mm. The dielectric substrate supporting the resistive sheet is a 0.5-mm-thick F4BM, whose relative permittivity ε_r is 2.65.

The bottom layer is a triple-layer CRSF. It consists of three metallic surfaces and two substrates. One substrate is double-side-printed, and the aperture surface and a patch surface are printed on each side of it. The other substrate is single-side-printed, with a patch surface printed on it.

Figure 5(b) shows the equivalent circuit model (ECM) of the proposed FSR. The meander lines are equal to an inductance in the lumped circuit, while the gaps between the units or meander lines are equivalent to the capacitances. By simulating the ECM using ADS, the correctness of ECM has been verified. The comparison of the transmission/reflection coefficient is shown in Fig. 6.

The simulated S-parameters of the proposed FSR under TE/TM-polarized oblique incidences are shown in Fig. 7. The 3 dB bandwidth is 2.7 GHz, which is from 7.5 to 10.2 GHz, and the fractional bandwidth is 30.5%, while the absorption band with the reflection coefficient less than −10 dB is from 2.4 to 6.2 GHz. The proposed FSR has a stable frequency response under 0–30 deg oblique incidences. However, as the structure of the meander line has a strong resonance, there is a thorn at 3.81 GHz for TE-polarization under oblique incidences when the incidence angle reaches 30 deg. $|S_{11}|$ of the thorn is
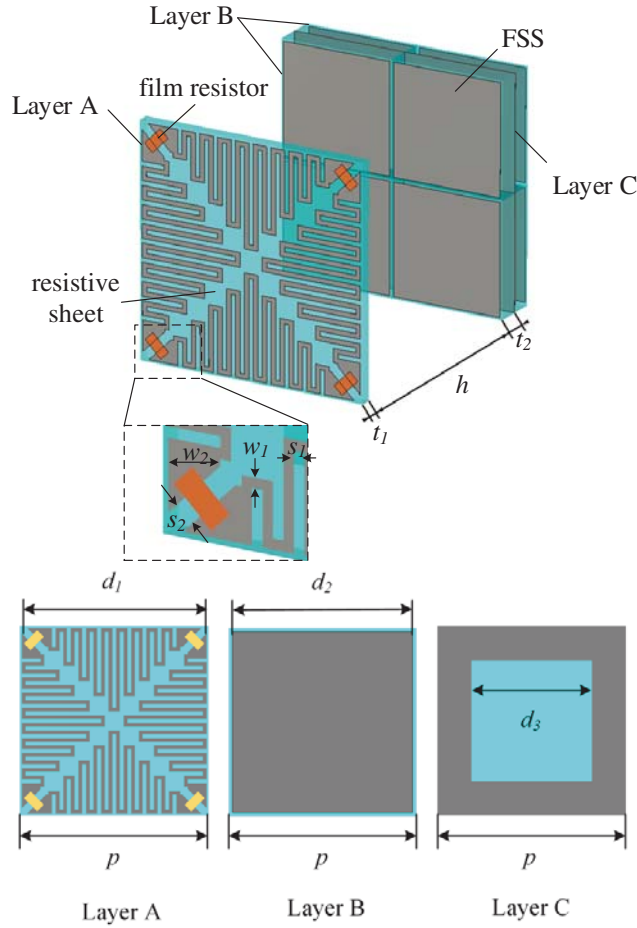
Figure 4. Geometric topology of the proposed FSR ($p = 10$ mm, $d_1 = 4.9$ mm, $d_2 = 4.8$ mm, $d_3 = 3.2$ mm, $t_1 = 0.5$ mm, $t_2 = 1$ mm, $h = 10.5$ mm, $w_1 = 0.2$ mm, $w_2 = 0.6$ mm, $s_1 = 0.2$ mm, $s_2 = 0.6$ mm).

from 3.7 to 3.8 GHz, and the maximum value of $|S_{11}|$ is -7.25 dB, while the maximum value of $|S_{21}|$ is less than -20 dB, which has almost no impact on the transmission performance. In general, the proposed FSR maintains a good frequency response performance.

3. FABRICATION AND MEASUREMENT

To validate the correctness of the simulated results in Section 2, a prototype was fabricated using printed circuit board (PCB) manufacturing process. The manufactured PCB is shown in Fig. 8. The resistive sheet was printed on a 0.5 mm-thick F4BM with immersion gold process. Four RC0402 chip resistors with values of 270 Ω were placed across the gap of the meander line. An SMT machine was used to weld the chip resistors onto the substrates, for convenience and a good performance consistency. The FSS was printed on a 1 mm thick F4BM with immersion silver process. One of the substrates was double-side printed, and the other was single-side printed. The substrates dimensions were 22 cm × 22 cm, and the relative dielectric constant of all the substrates was 2.65. The resistive sheet and CRSF were screwed together, with ten 1 mm-thick gaskets and a 0.5 mm-thick gasket in between to ensure the 10.5 mm thick air spacer.

The measurement setup is shown in Fig. 9. A numerical control rotary table was used to place the prototype and to precisely control the incidence angle. Broadband horn antennas (2–18 GHz) were used, supported by a tripod, to ensure that the two horns and the center of the prototype were on the

(a)   (b)
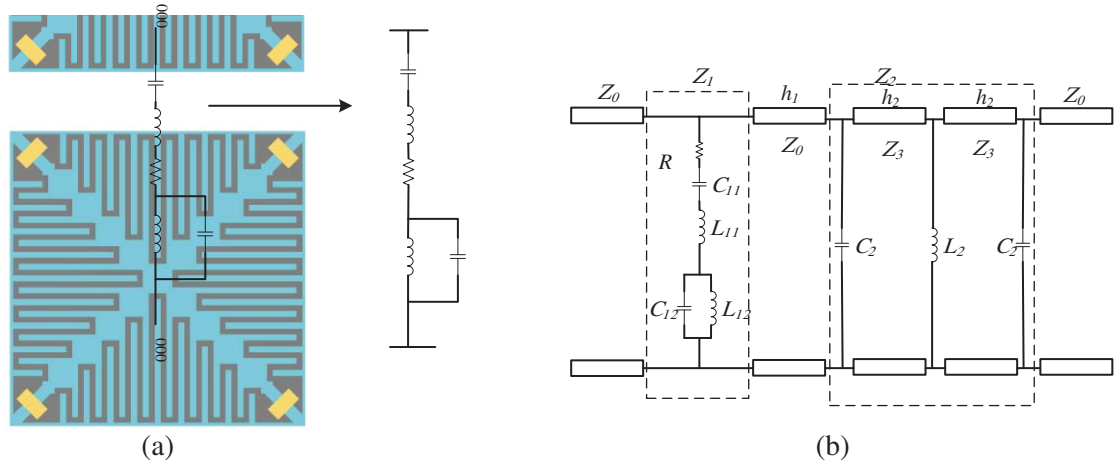
Figure 5. (a) Analysis of the resistive unit; (b) Equivalent circuit model of the proposed FSR ($R = 270\,\Omega$, $C_{11} = 4.418\,\mathrm{pF}$, $L_{11} = 12.8\,\mathrm{nH}$, $C_{12} = 3.416\,\mathrm{pF}$, $L_{12} = 2.267\,\mathrm{nH}$, $C_2 = 23.985\,\mathrm{pF}$, $L_2 = 0.135\,\mathrm{nH}$).

(a)   (b)
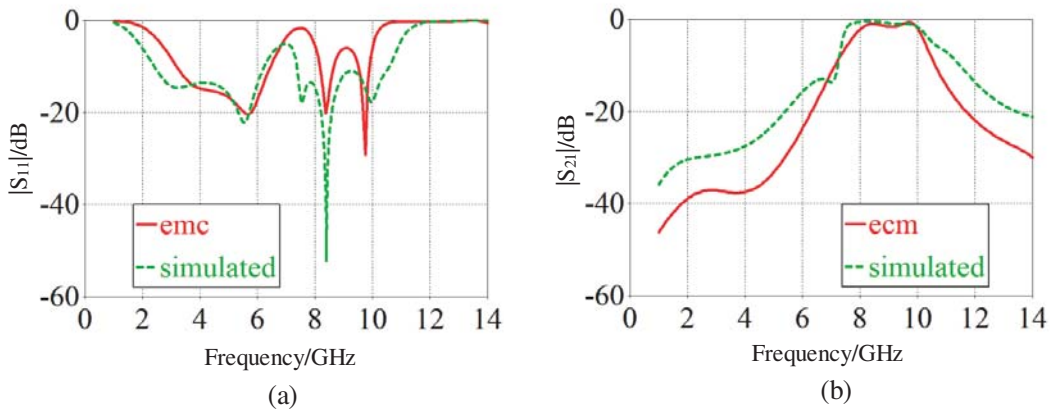
Figure 6. Comparison of the (a) transmission coefficient (b) reflection coefficient.

(a)   (b)   (c)   (d)
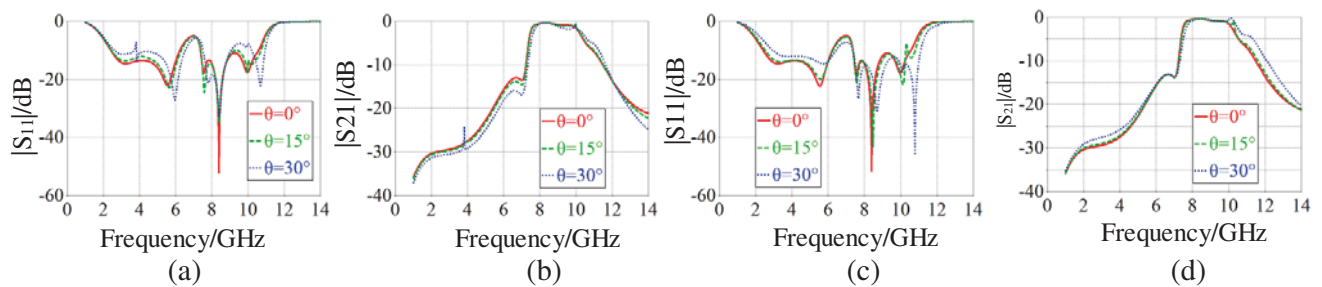
Figure 7. Frequency responses under oblique incidences: (a) transmission coefficient for TE-polarization; (b) reflection coefficient for TE-polarization; (c) transmission coefficient for TM-polarization; (d) reflection coefficient for TM-polarization.

same height. The N5524A vector network analyzer (VNA) was used for measurement from 2 to 40 GHz.

The comparison of the measured and simulated S-parameters is shown in Fig. 10. Under normal incidence, the measured 3 dB transmission band is 7.6–10.2 GHz, and the -10 dB absorption band is 3.0–6.4 GHz for TE-polarization. For TM-polarization, the 3 dB transmission band is 7.5–10.2 GHz, and
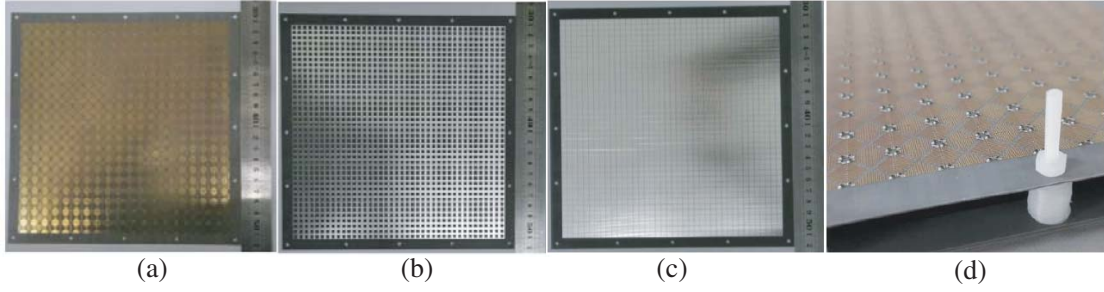
Figure 8. Manufactured prototype of the proposed FSR; (a) the resistive sheet; (b) the aperture array of the CRSF; (c) the patch array of the CRSF; (d) the integrated FSR.
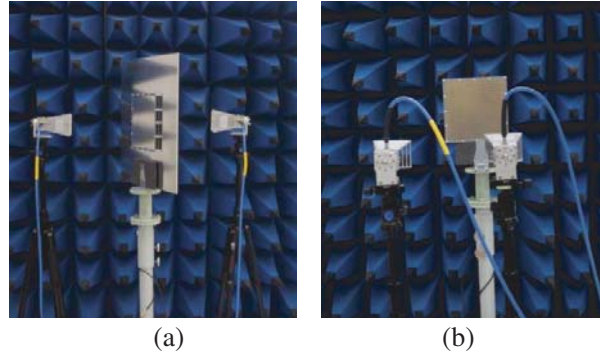
Figure 9. Measurement setup (a) for the manufactured prototype transmission coefficient; (b) for the manufactured prototype reflection coefficient.

Table 1. Comparisons (simulated results) between the proposed FSR and previously reported FSRS.

Ref.	A/T Location	Pass bandwidth, IL	Absorption bandwidth, IL	Passband (f_m), IL	Lumped elements in one unit	Polarization	Structure	Periodicity
[11]	A-T-A	N.A	79.3% + 29% (108.3%)	10.3 GHz, 0.3 dB	4	double	2-D	$0.19\lambda_L$
[19]	A-T-A	7.8% (5.43–5.87 GHz), 3 dB	90.6%	5.7 GHz, 0.48 dB	4	double	2-D	$0.234\lambda_L$
[20]	A-T-A	29% (4.45–5.96 GHz), 3 dB	41.3%+21.3% (62.6%)	5.3 GHz, 0.36 dB	8	double	2-D	$0.41\lambda_L$
[21]	T-A	25% (4.1–5.3 GHz), 1 dB	57.7%	N.A	8	double	2-D	$0.256\lambda_L$
[22]	A-T-A	23.6% (9.59–12.16 GHz), 3 dB	103%	10.28 GHz, 0.118 dB	2	double	2-D	$0.13\lambda_L$
Our work	A-T	30.5% (7.5-10.2 GHz), 3 dB	88.4%	8.3 GHz, 0.36 dB	4	double	2-D	$0.08\lambda_L$

IL = insertion loss, f_m = minimum IL frequency, λ_L = free-space wavelength at f_m; A-T = absorption band below the transmission band; A-T-A = two absorption bands around the transmission band.
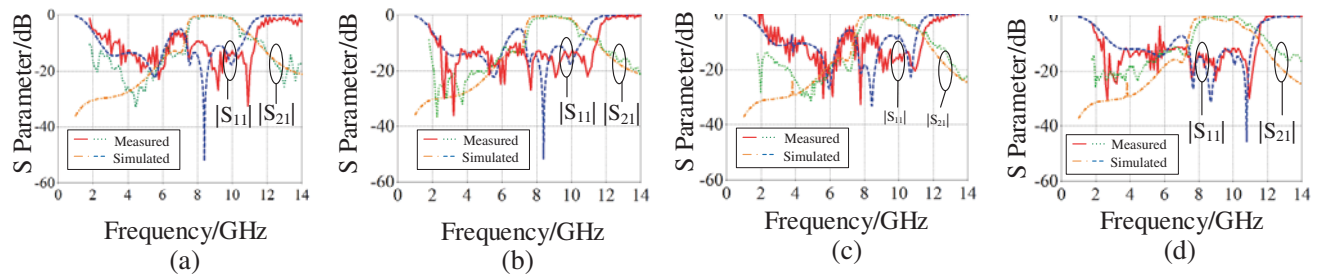
Figure 10. Comparison of measurement and simulation results (a) under normal incidence of TE-polarization; (b) under normal incidence of TM-polarization; (c) under the 30 deg. incidence of TE-polarization; (d) under the 30 deg. incidence of TM-polarization.

the -10 dB absorption band is 2.5–6.8 GHz. Under oblique incidence, the transmission coefficient and transmission coefficient for both TE-polarization and TM-polarization are maintained stable. As the two horns are close to each other when measuring the reflection coefficient, there is a strong coupling between them. The measured reflection coefficient has more intense oscillation than the simulated one. Because of diffraction, the measurement results at low frequency do not agree well with the simulation ones. Except these, simulated and measured results present good agreement.

To demonstrate the performance of the proposed FSR, the comparison with the recently published work is shown in Table 1. As illustrated in Table 1, the advantages of our work are smaller period, wider pass bandwidth, fewer lumped resistors, and simpler 2-D structure.

4. CONCLUSION

In this study, a miniaturized 2-D FSR is designed and fabricated for validation. The proposed FSR consists of a CRSF and a resistive sheet, which is a meander line loaded with film resistors. It has a wide transmission band (30.5%, 7.5–10.2 GHz) and a wide absorption band (88.4%, 2.4–6.2 GHz). Furthermore, the period of the FSR is only 10 mm ($0.08\lambda_L$), which is smaller than those of the most recently published works. The structure of proposed FSR could be used in future miniaturization applications. As the FSR combines the advantages of the FSS and the rasorber, it would be important in radome and other fields that need both stealth and filtering.

ACKNOWLEDGMENT

REFERENCES

1. Munk, B. A., *Frequency Selective Surfaces: Theory and Design*, Wiley, New York, 2000.

2. Narayan, S. and R. M. Jha, "Electromagnetic techniques and design strategies for FSS structure applications [antenna applications corner]," *IEEE Antennas and Propagation Magazine*, Vol. 57, No. 5, 135–158, Oct. 2015.

3. Pelton, E. L. and B. A. Munk, "A streamlined metallic radome," *IEEE Trans. Antennas Propag.*, Vol. 22, No. 6, 799–803, Nov. 1974.

4. Gerini, G. and L. Zappelli, "Multilayer array antennas with integrated frequency selective surfaces conformal to a circular cylindrical surface," *IEEE Trans. Antennas Propag.*, Vol. 53, No. 6, 2020–2030, Jun. 2005.

5. Xue, J., W. Jiang, and S. Gong, "Wideband RCS reduction of microstrip antenna based on 2.5-dimension miniaturized frequency selective surface," *2016 IEEE 5th Asia-Pacific Conference on Antennas and Propagation (APCAP)*, 209–210, Kaohsiung, 2016.

6. Leingthone, M. M. and N. Hakem, "A reconfigurable beam swhitching antenna using active cylindrical fss structure," *2017 IEEE International Symposium on Antennas and Propagation & USNC/URSI National Radio Science Meeting*, 2339–2340, San Diego, CA, 2017.

7. Sangeetha, B., G. Gulati, R. U. Nair, and S. Narayan, "Design of airborne radome using Swastika-shaped metamaterial-element based FSS," *2016 IEEE Annual India Conference (INDICON)*, 1–5, Bangalore, 2016.

8. Munk, B. A., *Metamaterials: Critique and Alternatives*, Wiley, New York, 2009.

9. Mantash, M., M. B. Kakhki, and T. A. Denidni, "Millimeter-wave circularly polarized vivaldi antenna using simple single layer 2D FSS polarizer," *2018 18th International Symposium on Antenna Technology and Applied Electromagnetics (ANTEM)*, 1–2, Waterloo, ON, 2018.

10. Mirza, H., et al., "Circuit model for a textile linear-to-circular polarizer using swastika-shaped FSS," *2019 URSI Asia-Pacific Radio Science Conference (AP-RASC)*, 1–4, New Delhi, India, 2019.

11. Chen, Q., D. Sang, M. Guo, and Y. Fu, "Frequency-selective rasorber with inter-absorption band transparent window and interdigital resonator," *IEEE Trans. Antennas Propag.*, Vol. 66, 4105–4114, 2018.

12. Chen, Q., D. Sang, M. Guo, and Y. Fu, "Miniaturized frequency-selective rasorber with a wide transmission band using circular spiral resonator," *IEEE Trans. Antennas Propag.*, Vol. 67, No. 2, 1045–1052, Feb. 2019.

13. Wang, Y., S. Qi, W. Wu, and Z. Shen, "An ultra-thin wideband 3-D frequency selective rasorber based on ferrite absorber and slow wave structure," *2019 IEEE International Symposium on Antennas and Propagation and USNC-URSI Radio Science Meeting*, 957–958, Atlanta, GA, USA, 2019.

14. Al-Joumayly, M. A. and N. Behdad, "A generalized method for synthesizing miniaturized element band-pass frequency selective surfaces," *2010 IEEE Antennas and Propagation Society International Symposium*, 1–4, Toronto, ON, 2010.

15. Han, M., M. He, H. J. Sun, K. Zhang, and G. Q. Zhao, "A frequency selective surface radome using a coupled resonator filter," *2013 IEEE International Conference on Microwave Technology & Computational Electromagnetics*, 52–54, Qingdao, 2013.

16. Luo, G. Q., W. L. Yu, and Y. F. Yu, "3D frequency selective rasorber with wide lower absorption band (invited)," *2017 Sixth Asia-Pacific Conference on Antennas and Propagation (APCAP)*, 1–3, Xi'an, 2017.

17. Xiu, X., W. Che, Y. Han, and W. Yang, "Low-profile dual-polarization frequency-selective rasorbers based on simple-structure lossy cross-frame elements," *IEEE Antennas and Wireless Propagation Letters*, Vol. 17, No. 6, 1002–1005, Jun. 2018.

18. Tuan, S., H. Chou, Y. Chang, H. Kun, P. Wang, and J. Zhang, "A practical microwave absorber design based on salisbury screens," *2016 International Symposium on Antennas and Propagation (ISAP)*, 944–945, Okinawa, 2016.

19. Qu, M., S. Sun, L. Deng, and S. Li, "Design of a frequency-selective rasorber based on notch structure," *IEEE Access*, Vol. 7, 3704–3711, 2019.

20. Xiu, X., Y. Han, W. Che, and W. Yang, "Double-polarization frequency selective rasorber based on cross-frame and circle ring slot arrays," *2017 10th Global Symposium on Millimeter-Waves*, 109–111, Hong Kong, 2017.

21. Wei, J., et al., "A wideband transmission frequency selective surface rasorber with low insertion loss," *2019 Thirteenth International Congress on Artificial Materials for Novel Wave Phenomena (Metamaterials)*, X-468–X-470, Rome, Italy, 2019.

22. Sun, Y., S. Xiao, Z. Yao, and Q. Shi, "A wideband frequency-selective rasorber based on interdigital resonator and fractal shaped slot," *2019 IEEE MTT-S International Wireless Symposium (IWS)*, 1–3, Guangzhou, China, 2019.

23. Kumar, A., D. K. Choudhary, and R. K. Chaudhary, "Metamaterial tri-band bandpass filter using meander-line with rectangular-stub," *Progress In Electromagnetics Research Letters*, Vol. 66, 121–126, 2017.

24. Choudhary, D. K. and R. K. Chaudhary, "Via-less wideband bandpass filter using CRLH transmission line with semi-circular stub," *2nd International Conference on Microwave and Photonics (ICMAP)*, Dec. 11–13, 2015.